

Effects of grain alignment with magnetic fields on grain growth and the structure of dust aggregates

THIEM HOANG,^{1,2}

¹*Korea Astronomy and Space Science Institute, Daejeon 34055, Republic of Korea, thiemhoang@kasi.re.kr*

²*Korea University of Science and Technology, 217 Gajeong-ro, Yuseong-gu, Daejeon, 34113, Republic of Korea*

ABSTRACT

Dust grains are aligned with the interstellar magnetic field and drift through the interstellar medium (ISM). Evolution of interstellar dust is driven by grain motion. In this paper, we study the effect of grain alignment with magnetic fields and grain motion on grain growth in molecular clouds. We first discuss characteristic timescales of internal alignment (i.e., alignment of the grain axis with its angular momentum, \mathbf{J}) and external alignment (i.e., alignment of \mathbf{J} with the magnetic field) and find the range of grain sizes that have efficient alignment. Then, we study grain growth for such aligned grains drifting through the gas. Due to the motion of aligned grains along the magnetic field, gas accretion would increase the grain elongation rather than decrease, as in the case of random orientation. Grain coagulation also gradually increases grain elongation, leading to the increase of elongation with the grain size. The coagulation of aligned grains can form dust aggregates that contain the elongated binaries comprising a pair of grains with parallel short axes. The presence of superparamagnetic iron clusters within dust grains enhances internal alignment and thus increases the maximum size of aligned grains from ~ 2 to $\sim 10 \mu\text{m}$ for dense clouds of $n_{\text{H}} \sim 10^5 \text{cm}^{-3}$. Determining the size of such aligned grains with parallel axes within a dust aggregate would be important to constrain the location of grain growth and the level of iron inclusions. We find that grains within dust aggregates in 67P/Churyumov-Gerasimenko obtained by *Rosetta* have the grain elongation increasing with the grain radius, which is not expected from coagulation by Brownian motion but consistent with the grain growth from aligned grains.

Keywords: ISM: dust-extinction, ISM: general, radiation: dynamics, polarization, magnetic fields

1. INTRODUCTION

Dust is an essential component of the interstellar medium (ISM) and plays an important role in various astrophysical processes, including star and planet formation, gas heating and cooling, formation of water and complex molecules, and planet formation. Dust is processed in the ISM due to gas-grain and grain-grain collisions. Grain growth by gas accretion is expected to occur in MCs where the visual extinction from the cloud surface of $A_V \gtrsim 3$ (Whittet et al. 1983), starting with the formation of an ice mantle on the grain core. Grain coagulation by grain-grain collisions is also found to be efficient in MCs. For instance, Ormel et al. (2009) suggested that dust coagulation can form micron-sized grains in MCs if the grains are coated with an ice mantle such that the sticking coefficient is enhanced, allowing grain growth upto the shattering threshold of $v_{\text{shat}} \sim 2.7 \text{km s}^{-1}$ (see also Hirashita & Li 2013).

The efficiency of grain growth essentially depends on the dust physical properties and grain motion. Grain

motion relative to the gas (e.g., drift) is common in the ISM due to various acceleration processes, including radiation pressure acceleration, magnetohydrodynamic (MHD) turbulence, shocks. For instance, charged dust grains can be accelerated by MHD turbulence through gyroresonance effect (Yan & Lazarian 2003; Yan et al. 2004) or transit time damping Hoang et al. (2012). The grain motion due to gyroresonance acceleration is important for grain coagulation and shattering by grain-grain collisions (Hirashita & Yan 2009; Hirashita et al. 2021).

Previous studies on grain growth usually ignore the effect of magnetic fields and assume spherical grains or randomly oriented grains. Nevertheless, dust grains in general have non-spherical shapes (e.g., elongated shape) and are systematically aligned with the magnetic field, as revealed by starlight polarization (Hall 1949; Hiltner 1949) and polarization of thermal dust emission (e.g., Planck Collaboration et al. 2015b). Moreover, modern theory based on Radiative Torques (RATs; Lazarian & Hoang 2007a; Hoang & Lazarian 2008) im-

plies that grain alignment with the magnetic field is efficient in most astrophysical environments, from the ISM to dense MCs (Hoang & Lazarian 2014; Hoang et al. 2021) where grain growth occurs efficiently. Indeed, multiwavelength polarization observations reveal that grains are still aligned at high extinction of $A_V > 20$ within dense clouds (Wang et al. 2017; Vaillancourt et al. 2020). Therefore, grain growth naturally involves aligned grains instead of randomly oriented grains. Because grains tend to align with their short axes perpendicular to the mean magnetic field (Lazarian et al. 2015), grain growth from collisions between aligned grains would be dramatically different from randomly oriented grains and would leave fundamental features in large composite particles.

Another interesting property of grain motion in the magnetized turbulent ISM is that grain acceleration by MHD turbulence is mostly perpendicular to the magnetic field because gyroresonance tends to increase the pitch angle between the grain motion and the magnetic field (Yan & Lazarian 2003; Yan et al. 2004). The effect of turbulence can induce the mixing, but the turbulence is for the bulk, not among the grains. In star-forming clouds, ambipolar diffusion also induces grain motion perpendicular to the ambient magnetic field. The direction of the grain's motion is therefore parallel to the grain long axis, and both are perpendicular to the magnetic field. This fundamental property may affect the shape of grains resulting from gas accretion and grain-grain collisions because the collisional cross-section becomes anisotropic. The main goal of this paper is to study the effect of grain alignment with the magnetic field on the grain shape and structure, and discuss the implications for observational constraints of dust physics.

The paper is organized as follows. In Section 2, we discuss the leading processes that induces the grain motion in perpendicular to the magnetic field. In Section 3, we discuss characteristic timescales relevant in grain alignment and identify the range of grain sizes that have efficient alignment with the magnetic field. In Sections 4 and 5, we study the grain growth due to gas accretion and grain-grain collisions for aligned grains, respectively. Discussion and summary of our main results are presented in Section 6 and 7, respectively.

2. GRAIN MOTION PERPENDICULAR TO THE MAGNETIC FIELD

We first discuss the main processes inducing grain motion in the direction perpendicular to the magnetic field, including gyroresonance acceleration, ambipolar diffusion, and shocks, as discussed in Lazarian (2020).

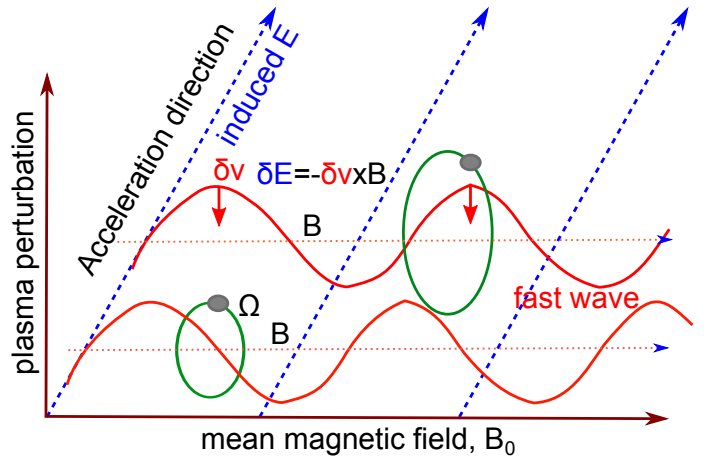


Figure 1. Illustration of grain acceleration by gyroresonance. A charged grain gyrates around the mean field (green loop). Fluctuations of fluid induced by fast modes induces an electric field $\delta\mathbf{E}$ perpendicular to the mean field, which accelerates charged grains in this direction.

2.1. Gyroresonance acceleration by MHD turbulence

MHD turbulence is found to efficiently accelerate charged grains. Figure 1 shows the schematic illustration of grain acceleration by gyroresonance, leading to the grain motion perpendicular to the mean magnetic field. The velocity of grains due to MHD acceleration is found to change with environments (Hoang et al. 2012).

For silicate grains in MCs, the grain velocity is approximated to be $v_d \sim 0.4 - 1 \text{ km s}^{-1}$ for $a > 0.05 \mu\text{m}$ and $v_d \sim (a/0.05 \mu\text{m})^{-3}$ for smaller grains. For dense clouds (DC), the grain velocity is smaller of $v_d \sim 0.3 - 1 \text{ km s}^{-1}$ for up to micron-sized grains. In the Cold Neutral Medium (CNM), grain velocity can reach $v_d \sim 1 \text{ km s}^{-1}$ (Yan et al. 2004). Note that, for a gas of temperature T_{gas} , the thermal velocity of gas atoms of mass m_{H} is $v_{\text{T}} = (2k_{\text{B}}T_{\text{gas}}/m_{\text{H}})^{1/2} \approx 0.4T_1 \text{ km s}^{-1}$ where $T_1 = T_{\text{gas}}/10 \text{ K}$. Thus, MHD turbulence can induce subsonic to supersonic motion of grains across the interstellar magnetic field.

2.2. Ambipolar diffusion

In star-forming magnetized MCs, such as dense cores or prestellar cores, charged grains are tied to the magnetic field but neutral gas can cross the field and collapses to form a protostar. The ambipolar diffusion results in the drift of grains in the direction perpendicular to the magnetic field. Gas accretion is then anisotropic similar to gyroresonance acceleration. The ambipolar diffusion velocity is 0.1 km s^{-1} , which is comparable to thermal speed in cold clouds. The magnetic field strength in dense MCs of $n_{\text{H}} > 300 \text{ cm}^{-3}$ is $B \approx 49(n_{\text{H}}/10^4 \text{ cm}^{-3})^{0.65} \mu\text{G}$, and $B \approx 5 \mu\text{G}$ for $n_{\text{H}} < 300 \text{ cm}^{-3}$ (Crutcher 2010).

2.3. Shocks in magnetized media

Shocks are present in dense MCs due to young stellar outflows. The shock can induce the grain motion perpendicular to the magnetic field. The idea is that charged grains gyrate around the magnetic field and tied to the field. Neutral gas-dust drag can then induce the grain motion across the magnetic field. The drift speed of dust relative to the neutral gas depends on the shock speed and the magnetic field strength and can reach supersonic (Hoang & Tram 2019).

3. GRAIN ALIGNMENT WITH MAGNETIC FIELDS

Grain alignment with the magnetic field can be distinguished into two stages: (i) the alignment of the grain axis of maximum inertia moment (shortest axis) parallel to its angular momentum, \mathbf{J} (hereafter internal alignment), and (ii) the alignment of \mathbf{J} with the magnetic field (hereafter external alignment; see Lazarian 2007; Lazarian et al. 2015 for recent reviews). When the internal alignment occurs with the axis of maximum inertia moment (shortest axis) perpendicular to \mathbf{J} , it is called *wrong internal alignment*. In this section, we review the main processes and show that micron-sized grains can be efficiently aligned in MCs.

3.1. Grain rotational damping

Let consider an oblate spheroidal grain of semi-major and semi-minor axis a and c , respectively, and let $s = c/a < 1$ be the axial ratio.

The rotational damping time due to gas collisions followed by evaporation is given by

$$\begin{aligned} \tau_{\text{gas}} &= \frac{3}{4\sqrt{\pi}} \frac{I_{\parallel}}{1.2n_{\text{H}}m_{\text{H}}v_{\text{th}}a^4\Gamma_{\parallel}} \\ &\simeq 8.3 \times 10^3 \hat{\rho} a_{-5} \left(\frac{1}{n_3 T_1^{1/2} \Gamma_{\parallel}} \right) \text{ yr}, \end{aligned} \quad (1)$$

where $I_{\parallel} = 8\pi\rho sa^5/15$, $a_{-5} = a/(10^{-5} \text{ cm})$, $\hat{\rho} = \rho/(3 \text{ g cm}^{-3})$ with ρ being the dust mass density, and Γ_{\parallel} is the geometrical factor of unity order (Hoang & Lazarian 2009b). The gas temperature and gas density are normalized to their typical values of a dense MC with $n_3 = n_{\text{H}}/(10^3 \text{ cm}^{-3})$, respectively.

3.2. Internal Alignment: Barnett Relaxation

Silicate grains or dust grains with iron inclusions are paramagnetic material due to the existence of unpaired electrons. A rotating paramagnetic grain can thus acquire a magnetic moment thanks to the Barnett effect (see Barnett 1915; Landau & Lifshitz 1969) and the rotation of its charged body (Martin 1972; Dolginov &

Mytrophanov 1976). The Barnett effect, which is shown to be much stronger than the latter, induces a magnetic moment proportional to the grain angular velocity:

$$\boldsymbol{\mu}_{\text{Bar}} = -\frac{\chi(0)V\hbar}{g_e\mu_B}\boldsymbol{\omega}, \quad (2)$$

where $V = 4\pi sa^3/3$ is the grain volume, $\chi(0)$ is the grain magnetic susceptibility at rest, the gyromagnetic ratio $g_e \approx 2$ for electrons, and $\mu_B = e\hbar/2m_e c$ is the Bohr magneton (see Draine 1996 and references therein).

The magnetic susceptibility for paramagnetic grains at dust temperature T_d is given by

$$\chi(0) \simeq 0.06 f_p \hat{n}_{23} \hat{p}^2 \left(\frac{10 \text{ K}}{T_d} \right), \quad (3)$$

where $\hat{n}_{23} = n/10^{23} \text{ cm}^{-3}$ is the atomic density of material, f_p is the fraction of paramagnetic (Fe) atoms in the dust grain. Above, $\hat{p} = p/5.5$ with $p = g_e \sqrt{J(J+1)}$ with J the angular momentum quantum number of electrons in the outer partially filled shell. For silicate of MgFeSiO_4 , $f_p = 1/7$ and $J = 5/2$ (see Hoang & Lazarian 2016).

Grains having embedded iron cluster become superparamagnetic material because the iron clusters act as giant magnetic moment. The magnetic susceptibility is enhanced significantly to:

$$\chi_{\text{sp}}(0) \approx 0.052 N_{\text{cl}} \phi_{\text{sp}} \hat{p}^2 \left(\frac{10 \text{ K}}{T_d} \right). \quad (4)$$

A rotating paramagnetic grain experiences internal dissipation of energy due to Barnett relaxation (see Purcell 1979), which results in the alignment of the grain axis of major inertia (short axis) with the angular momentum (so-called internal alignment). The Barnett relaxation time is given by

$$\tau_{\text{Bar}} \approx 0.5 \hat{\rho}^2 a_{-5}^7 \hat{s} \left(\frac{1 + \hat{s}^2}{2} \right)^2 \left(\frac{\omega_d}{\omega} \right)^2 \left[1 + \left(\frac{\omega \tau_2}{2} \right)^2 \right]^2 \text{ yr}, \quad (5)$$

where $\hat{s} = s/0.5$, $\tau_2 \approx 2.9 \times 10^{-12} f_p^{-1} \text{ s}$ is the spin-spin relaxation time where the fraction of paramagnetic (Fe) atoms in the dust grain $f_p = 0.1$; $\omega_d = \sqrt{k_{\text{B}} T_d / I_{\parallel} (h-1)}$ is the dust thermal angular velocity with $h = I_{\perp} / I_{\parallel}$.

The Barnett relaxation time is much shorter than the gas rotational damping time, t_{gas} . Therefore, internal alignment is quickly established, resulting in the alignment of the short axis with the angular momentum.

The Barnett relaxation time for superparamagnetic grains is reduced by a factor N_{cl} :

$$\tau_{\text{Bar,sp}} \approx 3.2 \hat{\rho}^2 a_{-5}^7 \frac{1}{N_{\text{cl}}} \left(\frac{\omega_d}{\omega} \right)^2 \times \left[1 + \left(\frac{\omega \tau_{\text{sp}}}{2} \right)^2 \right]^2 \text{ yr}, \quad (6)$$

which is a factor $\sim N_{\text{cl}}$ smaller than the usual Barnett relaxation time.

Another internal relaxation is nuclear relaxation introduced by Lazarian & Draine (1999), which is important for large grains (Lazarian & Hoang 2008). The time scale for the nuclear relaxation for a "brick" with dimensions $a \times a\sqrt{3} \times a\sqrt{3}$ is:

$$\tau_{\text{nucl}} = G_{\text{nucl}} \hat{\rho}^2 a_{-5}^7, \quad (7)$$

where

$$G_{\text{nucl}} = 610 \left(\frac{n_e}{n_n} \right) \left(\frac{\omega_d}{\omega} \right)^2 \left(\frac{g_n}{3.1} \right) \left(\frac{2.7\mu_N}{\mu_n} \right) \left[1 + (\omega\tau_n/2)^2 \right]^2 \text{ s}, \quad (8)$$

where, $\hat{\rho} \equiv \rho/(2g \text{ cm}^{-3})$, n_e and n_n are the number density of nucleon and electron in the dust, the nuclear spins with magnetic moments $\mu_n = g_n\mu_N$ are normalized by the magnetic moment of the proton $\mu_N \equiv 5.05 \times e\hbar/2m_p c = 10^{-24} \text{ erg G}^{-1}$, τ_n is the time of spin-spin relaxation within the system of nuclear spins (see Lazarian & Hoang 2019).

3.3. External Alignment

3.3.1. Larmor precession

The interaction of the grain magnetic moment (Eq. 2) with the external static magnetic field, governed by the torque $[-\boldsymbol{\mu}_{\text{Bar}} \times \mathbf{B}] = -\mu_{\text{Bar}} B \sin \xi \hat{\phi}$, causes the regular precession of the grain angular momentum around the magnetic field direction. The rate of such a Larmor precession denoted by τ_{Lar} , is given by

$$\begin{aligned} \tau_{\text{Lar}} &= \frac{2\pi}{d\phi/dt} = \frac{2\pi I_{\parallel} \omega}{\mu_{\text{Bar}} B}, \\ &= 8.4 \hat{\rho}^{-1/2} \hat{\chi}^{-1} \hat{B}^{-1} a_{-5}^2 \text{ yr}, \end{aligned} \quad (9)$$

where $\hat{B} = B/5\mu\text{G}$ and $\hat{\chi} = \chi(0)/10^{-4}$ are the normalized magnetic field and magnetic susceptibility, respectively. For superparamagnetic grains, the Larmor timescale, $\tau_{\text{Lar,sp}}$, is given by the same formula but $\chi(0)$ is replaced by χ_{sp} (Eq. 4).

3.3.2. Paramagnetic and superparamagnetic relaxation

Rotating paramagnetic grains subject to an external magnetic field experiences magnetic relaxation that eventually leads to the alignment of the grain angular momentum, magnetic moment, and the magnetic field (Davis & Greenstein 1951). The characteristic time of the magnetic relaxation is given by

$$\begin{aligned} \tau_{\text{mag}} &= \frac{I_{\parallel}}{K(\omega) V B^2} = \frac{2\rho a^2 s^{-2/3}}{5K(\omega) B^2}, \\ &\simeq 2.4 \times 10^6 \hat{\rho} \hat{s}^{-2/3} a_{-5}^2 \hat{B}^{-2} \hat{K}^{-1} \text{ yr}, \end{aligned} \quad (10)$$

where $\hat{K} = K(\omega)/(10^{-13} \text{ s})$ and $K(\omega) = \chi_2(\omega)/\omega$ with $\chi_2(\omega)$ is the imaginary part of complex magnetic susceptibility of the grain material.

For paramagnetic grains, the frequency dependence susceptibility $K(\omega)$ can be described by critically-damped solution (Draine & Lazarian 1999)

$$\begin{aligned} K(\omega) &= \frac{\chi(0)\tau_2}{[1 + (\omega\tau_2/2)^2]^2} \\ &\simeq 8.7 \times 10^{-14} \hat{\rho} \left(\frac{20\text{K}}{T_d} \right) \frac{1}{[1 + (\omega\tau_2/2)^2]^2} \text{ s}. \end{aligned} \quad (11)$$

For superparamagnetic grains, the frequency dependence susceptibility $K_{\text{sp}}(\omega)$ is given by (see Hoang & Lazarian 2016):

$$\begin{aligned} K_{\text{sp}}(\omega) &= \frac{\chi_{\text{sp}}(0)\tau_{\text{sp}}}{[1 + (\omega\tau_{\text{sp}}/2)^2]^2}, \\ &\simeq 2.6 \times 10^{-11} N_{\text{cl}} \phi_{\text{sp}} \hat{\rho}^2 \frac{\exp(N_{\text{cl}} T_{\text{act}}/T_d)}{\hat{T}_d [1 + (\omega\tau_{\text{sp}}/2)^2]^2} \text{ s}, \end{aligned} \quad (12)$$

where τ_{sp}^{-1} is the rate of thermally activated remagnetization given by

$$\tau_{\text{sp}}^{-1} \approx \nu_0 \exp\left(-\frac{N_{\text{cl}} T_{\text{act}}}{T_d}\right) \quad (13)$$

where experiments give $\nu_0 \approx 10^9 \text{ s}^{-1}$ and $T_{\text{act}} \approx 0.011 \text{ K}$ (see Morrish 2001).

Plugging $K(\omega)$ and $K_{\text{sp}}(\omega)$ into Equation (10) one obtains the timescales of alignment by magnetic relaxation for paramagnetic and superparamagnetic material, which are denoted by $\tau_{\text{mag,PM}}$ and $\tau_{\text{mag,SPM}}$, respectively.

3.3.3. Radiative Torque (RAT) Alignment

Grains are spun-up by RATs to suprathreshold rotation. Due to grain suprathreshold rotation, efficient internal relaxation (Barnett and nuclear effects) quickly induces the alignment of the grain short axis with its angular momentum. Modern theory based on RATs implies that grain alignment with its angular momentum parallel to the magnetic field, resulting in the alignment of the short axis with the magnetic field (see Lazarian et al. 2015).

Numerical simulations show that grains can be efficiently aligned by RATs when they can rotate suprathresholdly (Hoang & Lazarian 2008; Hoang & Lazarian 2016). Taking the suprathreshold condition that corresponds to the grain angular momentum spun-up by RATs, ω_{RAT} , equal three times of its thermal value (i.e., $\omega_{\text{RAT}} = 3\omega_T = 3(kT_{\text{gas}}/I_{\parallel})^{1/2}$), one can determine the minimum size of grains that can be efficiently aligned

by RATs. For a starless MC, Hoang et al. (2021) derived the minimum size of aligned grains by interstellar radiation field (ISRF) as follows:

$$a_{\text{align}} = \left(\frac{1.2n_{\text{H}}T_{\text{gas}}}{\gamma u_{\text{rad}}\bar{\lambda}^{-2}} \right)^{2/7} \left(\frac{15m_{\text{H}}k^2}{4\rho} \right)^{1/7} \\ \simeq 0.055\hat{\rho}^{-1/7} \left(\frac{\gamma_{-1}U}{n_3T_1} \right)^{-2/7} \left(\frac{\bar{\lambda}}{1.2\mu\text{m}} \right)^{4/7} \mu \quad (14)$$

where $U = u_{\text{rad}}/u_{\text{MMP83}}$ is the ratio of the radiation energy density u_{rad} relative to that of the local ISRF in the solar neighborhood, u_{MMP83} (Mathis et al. 1983), $\bar{\lambda}$ is the mean wavelength of the local radiation field, and the damping due to infrared emission has been disregarded for starless dense clouds.

Equation (14) implies $a_{\text{align}} \sim 0.055, 0.21, 0.4\mu\text{m}$ for a dense cloud of $n_{\text{H}} = 10^3, 10^5, 10^6\text{cm}^{-3}$ exposed to the local radiation field of $\gamma = 0.1$, $U = 1$, and $\bar{\lambda} = 1.2\mu\text{m}$. Accounting for the attenuation of ISRF toward the MC center, calculations in Hoang et al. (2021) find that, at $A_V \sim 20$, the grain alignment size increases to $a_{\text{align}} \sim 0.3, 0.7, 1.5\mu\text{m}$, for $n_{\text{H}} \sim 10^4, 10^5, 10^6\text{cm}^{-3}$. Therefore, the grain coagulation to micron sizes in dense MC essentially involves aligned grains. For grains smaller than a_{align} , the coagulation can first occur for random grains and then become aligned by RATs when becoming larger than a_{align} .

The time required to spin-up grains to suprathermal rotation threshold is given by

$$\tau_{\text{spin-up}} \equiv \frac{3I_{\parallel}\omega_T}{\Gamma} = \frac{3\tau_{\text{drag}}}{\omega_{\text{RAT}}/\omega_T}, \\ \simeq \frac{2 \times 10^3 a_{-5} n_3^{-1} T_1^{1/2} yr}{(J_{\text{RAT}}/3J_{\text{th}})}, \quad (15)$$

Γ is the radiative torque magnitude (Draine & Weingartner 1996; Lazarian & Hoang 2007a), and $\omega_{\text{RAT}} = \Gamma\tau_{\text{gas}}/I_{\parallel}$ is the maximum angular momentum spun up by RATs.

For grains of $a = a_{\text{align}}$ with $\omega_{\text{RAT}} = 3\omega_T$, the RAT alignment timescale is comparable to τ_{gas} , and for $a > a_{\text{align}}$, the RAT alignment is then much shorter because those grains rotate suprathermally with $\omega_{\text{RAT}} > 3\omega_{\text{th}}$.

3.3.4. Mechanical Torque (MET) Alignment

Grains drifting through the gas experience mechanical torques (METs). As shown in Lazarian & Hoang (2007b) and Hoang et al. (2018), METs can efficiently align grains with the magnetic field, in analogy to RATs, i.e., the grain short axis is parallel to the magnetic field when internal relaxation is efficient. For inefficient internal relaxation, grain alignment can occur with the long axis parallel to the magnetic field.

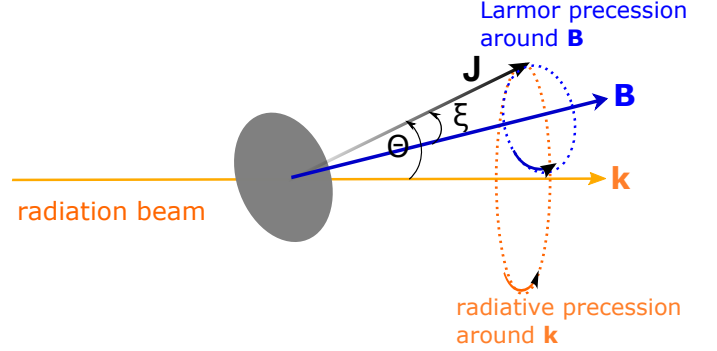


Figure 2. Schematic illustration of the precession of the grain angular momentum (\mathbf{J}) around the radiation direction (\mathbf{k}) and the magnetic field (\mathbf{B}), assuming the perfect internal alignment of the grain short axis with \mathbf{J} . The grain magnetic moment is directed along the angular momentum, \mathbf{J} . The fastest precession establishes the alignment axis by RATs.

3.4. Maximum grain sizes for internal and external alignment

Table 1. Physical parameters of the molecular clouds

Parameters	MC	DC
Gas density, $n_{\text{H}} (\text{cm}^{-3})$	10^3	10^5
Gas temperature, $T_{\text{gas}} (\text{K})$	15	10
Dust temperature, $T_{\text{d}} (\text{K})$	15	10
Magnetic field strength, $B (\mu\text{G})$	10	200
Gas Thermal speed, v_T	0.50	0.41
Grain drift velocity, $v_d (\text{km s}^{-1})$	0.5	0.5

Figure 3 shows the different timescales involved in grain alignment for the MC (left panel) and DC (right panel) with physical parameters shown in Table 1.

The internal alignment is established whenever $\tau_{\text{int}} < \tau_{\text{gas}}$, and external alignment with the magnetic field is achieved when $\tau_{\text{Lar}} < \tau_{\text{gas}}$. Barnett relaxation for grains with iron inclusions (super Barnett) of $N_{\text{cl}} = 10^4$ has shortest internal relaxation timescale, while ordinary paramagnetic Barnett relaxation is faster than the gas damping only for $a < 0.5\mu\text{m}$. Nuclear relaxation is more efficient than Barnett effect for large grains. Larmor precession is always faster than the gas damping time, such that the magnetic field determines the axis of external alignment. Timescale for paramagnetic relaxation is longer than the gas damping time, but superparamagnetic relaxation is shorter. One can see that alignment of short axis with the magnetic field occurs

for grains with iron inclusions of $a \lesssim 1 \mu\text{m}$ in MC and DC.

As the grain size increases, the internal relaxation rate decreases significantly as a^7 (see Eq. 5). Thus, it is important to estimate the maximum size below which internal relaxation is still efficient to induce internal alignment. For grains with iron inclusions, from Equations (1) and (6), it is straightforward to obtain the ratio of the Barnett relaxation to the gas damping time:

$$\frac{\tau_{\text{Bar,sp}}}{\tau_{\text{gas}}} = \frac{\gamma_e^2 n_{\text{H}} m v_{\text{th}} a \Gamma_{\parallel}}{s^{4/3} h^2 (h-1) \omega^2} \times \frac{[(1 + (\omega \tau_{\text{sp}}/2)^2)^2]}{\chi_{\text{sp}}(0) \tau_{\text{sp}}}, \quad (16)$$

$$= 8.5 \times 10^{-4} \frac{n_5 a^6 \Gamma_{\parallel}}{N_{\text{cl},4} \phi_{\text{sp},-2} \exp(N_{\text{cl}} T_{\text{act}}/T_d)} \quad (17)$$

where $h = 2$ is taken for the estimate. The maximum size for internal alignment is determined by $\tau_{\text{Bar,sp}}/\tau_{\text{gas}} < 1$, yielding

$$a_{\text{max,int}} < 1.8 \left(\frac{n_5 T_1^{-1/2}}{N_{\text{cl},5} \phi_{\text{sp},-2}} \right)^{-1/6} \left(\frac{[(1 + (\omega \tau_{\text{sp}}/2)^2)^2]}{\exp(N_{\text{cl}} T_{\text{act}}/T_d)} \right)^{-1/6} \times \left(\frac{\omega}{\omega_T} \right)^{1/3} \mu\text{m}, \quad (18)$$

which implies $a_{\text{max,int}} \approx 1.8 \mu\text{m}$ for $N_{\text{cl}} \sim 10^4$.

For large grains, nuclear relaxation becomes more efficient than Barnett relaxation. Thus, grains of size $a < a_{\text{max,int}}$ can have efficient internal alignment, leading to the alignment of the grain short axis along the magnetic field. However, large grains of size $a > a_{\text{max,int}}$ have inefficient internal alignment, leading the alignment with their short axes perpendicular to the magnetic field, (i.e., *wrong alignment*) (Hoang & Lazarian 2009a).

Figure 4 shows the variation of the maximum size of grains that can be aligned by Barnett relaxation, $a_{\text{max,int}}$, on the gas density for superparamagnetic grains of varying N_{cl} . The results for ordinary paramagnetic material are also shown in dotted lines (Barnett) and Barnett plus nuclear relaxation. For dense clouds of $n_{\text{H}} \lesssim 10^5 \text{cm}^{-3}$, internal alignment occurs for grains of sizes $a < a_{\text{max,int}} \sim 5 \mu\text{m}$, assuming $N_{\text{cl}} \lesssim 10^4$. In PPDs where the gas density in the disk interior is of $n_{\text{H}} \gtrsim 10^{10} \text{cm}^{-3}$, only small grains of $a < a_{\text{max,int}} \lesssim 0.5 \mu\text{m}$ can have internal alignment with their short axis parallel to the magnetic field. For ordinary paramagnetic dust, the maximum size by Barnett relaxation is much smaller than that due to nuclear relaxation because the latter is several orders more efficient, leading to the efficient internal alignment of $a_{\text{max,int}} \lesssim 2 \mu\text{m}$ for $n_{\text{H}} \gtrsim 10^3 \text{cm}^{-3}$.

We now estimate the maximum size of grains that still have external alignment with the magnetic field.

Using the Larmor precession time from Equation (9), one obtains the ratio of the Larmor precession to gas damping time:

$$\frac{\tau_{\text{Lar,sp}}}{\tau_{\text{gas}}} = \left(\frac{\tau_{\text{Lar,sp}}}{\tau_{\text{mag}}} \right) \left(\frac{\tau_{\text{mag}}}{\tau_{\text{gas}}} \right) = \frac{2\pi g_e \mu_B}{\hbar} \left(\frac{n_{\text{H}} m_{\text{H}} v_{\text{th}} \Gamma_{\parallel} a_2}{\chi_{\text{sp}}(0) s B} \right), \quad (19)$$

$$\simeq 0.02 \frac{n_5 T_2^{1/2} a_{-5} \Gamma_{\parallel}}{N_{\text{cl}} \phi_{\text{sp},-2} B_3},$$

where $n_5 = n_{\text{H}}/10^5 \text{cm}^{-3}$, $\phi_{\text{sp},-2} = \phi_{\text{sp}}/0.01$, and $B_3 = B/1000 \mu\text{G}$.

The maximum grain size that can be aligned with the magnetic field is then determined by $\tau_{\text{Lar,sp}}/\tau_{\text{gas}} < 1$, yielding

$$a_{\text{max,B}} < 1.4 \times 10^3 \frac{N_{\text{cl},4} \phi_{\text{sp},-2}}{n_5 T_1^{1/2} B_3 \Gamma_{\parallel}} \text{cm}, \quad (20)$$

where N_{cl} spans ~ 20 to 10^5 (Jones & Spitzer 1967). The equation implies that very large grains of 1000 cm can still be aligned with the magnetic field in dense clouds of $n_{\text{H}} \sim 10^5 \text{cm}^{-3}$. However, in the region of high density $n_{\text{H}} \sim 10^{12} \text{cm}^{-3}$ like PPDs, only large grains upto $a_{\text{max,B}} \sim 1 \mu\text{m}$ can be aligned with the magnetic field, assuming $N_{\text{cl}} \sim 10^4$.

Therefore, grain growth from interstellar grains of $a \sim 0.1 \mu\text{m}$ to micron-sized grains involve aligned grains.

4. GRAIN GROWTH BY GAS ACCRETION TO DRIFTING ALIGNED GRAINS

Suppose that the tiny grain drifts through the gas with a velocity v_d . Gas includes H, He and heavy elements (X) with $X = \text{C}, \text{O}, \text{Mg}, \text{Si}, \text{Fe}$. In MCs, the accretion of H leads to formation of H_2 and water ice mantle in which most of H_2 molecules rapidly desorb. Gas accretion then gradually increases the grain size to $a > a_{\text{align}}$. Note that accretion of H quickly evaporate and thus does not raise the grain mass. Afterward, the gas accretion now acts on the grain that is aligned with the short axis parallel to the magnetic field.

Let $\hat{x}\hat{y}\hat{z}$ be the lab frame in which \hat{z} is chosen to be along the magnetic field, \mathbf{B} . The grain drift velocity is assumed to be along \hat{x} axis, and $\mathbf{v}_d = v_d \hat{x}$. Let $s_d = v_d/v_T$ with $v_T = (2kT_{\text{gas}}/m_{\text{H}})^{1/2}$.

4.1. Non-aligned grains

We first consider the accretion of the gas to a tiny, randomly oriented grain of size $a < a_{\text{align}}$. Since the drift velocity of tiny grains by MHD turbulence is small (subsonic), one can ignore the drift. Due to randomization by gas collision, the gas accretion to the grain leads to isotropic increase in the grain size. The accretion rate

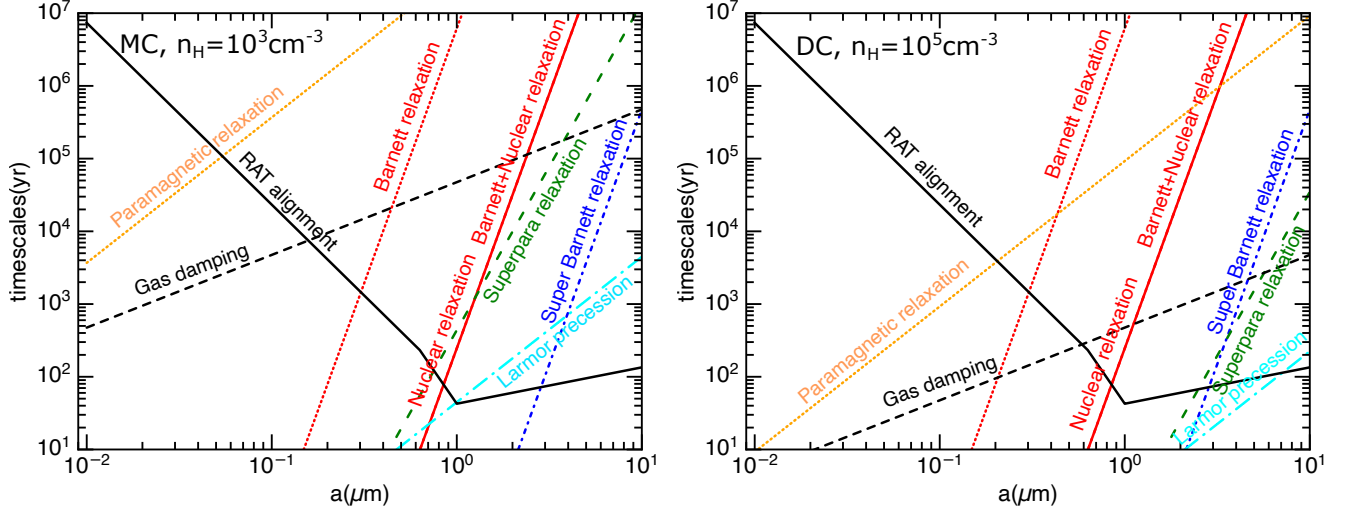


Figure 3. Characteristic timescales of various processes in grain alignment for the MC of $n_{\text{H}} = 10^3 \text{ cm}^{-3}$ (left panel) and $n_{\text{H}} = 10^5 \text{ cm}^{-3}$ (right panel). Barnett relaxation for superparamagnetic grains with iron inclusions of $N_{\text{cl}} = 10^4$ has a shortest timescale, while ordinary Barnett relaxation is faster than the gas damping for $a < 0.5 \mu\text{m}$. Larmor precession is always faster than the gas damping time which makes the grain alignment with respect to the magnetic field.

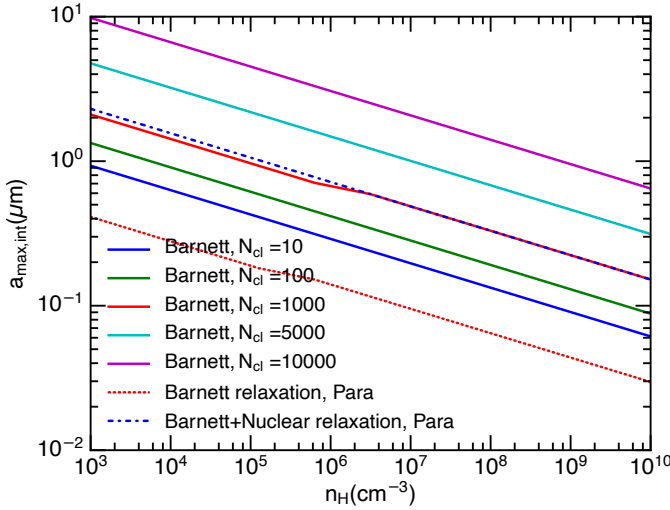


Figure 4. Maximum grain size for efficient internal alignment with the grain short axis parallel to the magnetic field by Barnett relaxation and nuclear relaxation as a function of the local gas density. Grains larger than $a_{\text{max,int}}$ have wrong internal alignment with their long axes parallel to the magnetic field. Different levels of iron inclusions described by N_{cl} is considered.

of the element x to the grain is then given by the same formulae as the gas accretion onto a spherical grain:

$$\frac{dm_{\text{gr}}}{dt} = \sum_X m_x n_x \langle v \rangle_x \pi a^2 S_x. \quad (21)$$

where S_x is the sticking coefficient, $\langle v \rangle_x = (8kT_{\text{gas}}/\pi m_x)^{1/2} \simeq 0.46 T_1^{1/2} M_x^{-1/2} \text{ km/s}$ where $T_1 = T_{\text{gas}}/10 \text{ K}$ is the mean thermal speed and M_x is the

atomic mass in amu, and the summation is carried over all heavy elements (X).

The increase in the grain size by gas accretion is

$$\frac{da}{dt} = \frac{3 \sum_X m_x n_x \langle v \rangle_x \pi a^2 S_x}{4\pi a^2 \rho} \quad (22)$$

The accretion time to increase the grain size by a thickness of a is

$$\begin{aligned} \tau_{\text{acc}} &= \frac{a}{da/dt} = \frac{4a\rho}{3\mu m_{\text{H}} n_{\text{H}} \langle v \rangle X} \\ &\simeq 1.2 \times 10^6 \frac{\hat{\rho} a_{-5}}{n_3 T_1^{1/2} X_{-2}} \text{ yr}, \end{aligned} \quad (23)$$

where $\mu = 1.4$ is the mean molecular weight of the gas with 10% mass from He, and the mass fraction of heavy elements is normalized to its typical mass of the ISM with $X = \rho_X/\rho_{\text{gas}} = 10^{-2}$ with $\rho_{\text{gas}} = \mu m_{\text{H}} n_{\text{H}}$.

Equation (23) reveals that the grain can grow to two its original size within 1 Myr. Over the time of the universe of 10 Gyr, the grain growth by gas accretion could be very large if there are no destructive processes such as shattering and rotational disruption by RATs (RATD, Hoang et al. 2019).

4.2. Aligned grains

We now discuss the accretion to aligned grains that have sizes $a_{\text{align}} < a < a_{\text{max,int}}$. Due to fast spinning along the short axis, the grain can be approximated as an oblate spheroid with the length of the semi-major and minor axes denoted by a and $c < a$, respectively. For simplicity, we assume that grain alignment is perfect with the short axis is parallel to the angular momentum

\mathbf{J} and along the magnetic field. Because the rotation period is much shorter than the mean time between two gas-grain collisions, the geometrical cross-section of the frontal surface is πac and of the perpendicular surface πa^2 .

The collision rate of the gas specie X to the grain along the direction of the motion is (see Appendix A):

$$F_z = \frac{1}{4} n_X \langle v \rangle_X, \quad (24)$$

$$F_y = \frac{1}{4} n_X \langle v \rangle_X, \quad (25)$$

$$F_x = \frac{1}{4} n_X \langle v \rangle_X \left(e^{-s_d^2} + \sqrt{\pi} s_d [1 + \text{erf}(s_d)] \right), \quad (26)$$

which yields

$$\frac{F_x}{F_y} = \left(e^{-s_d^2} + \sqrt{\pi} s_d [1 + \text{erf}(s_d)] \right) \quad (27)$$

For $s_d \gg 1$, the second term of Equation (26) dominates $F_x/F_y \rightarrow 2\sqrt{\pi} s_d = v_d/v_T$. For $s_d = 0$, one has $F_x/F_y = 1$.

Figure 5 shows the rapid increase of F_x/F_z with the ratio of the drift speed relative to the thermal speed, v_d/v_T . If the grain drifts at speed of $s_d = 0.5$, the head-on collision rate is five time greater than the collision rate along the magnetic field (red line).

For the gas of H and He only, the rate of the increase in the grain mass by accretion along the direction of the motion is

$$\begin{aligned} \frac{dm_x}{dt} &= \mu m_H F_x \pi a c S_X \\ &= \frac{1}{4} S n_H \mu m_H \pi a c \langle v \rangle \left(e^{-s_d^2} + \sqrt{\pi} s_d [1 + \text{erf}(s_d)] \right) \end{aligned} \quad (28)$$

where S is the sticking coefficient.

The rate of the increase in the grain mass by accretion along the direction perpendicular to the direction of grain motion is

$$\frac{dm_z}{dt} = \mu m_H F_z \pi a^2 S = \frac{1}{4} \mu m_H S n_H \pi a^2 \langle v \rangle. \quad (29)$$

Assuming that initial grain shape is slightly elongated with $a \approx c$, the new axial ratio of the grain after a time Δt is then

$$\frac{a_{\text{new}}}{c_{\text{new}}} = \frac{a + \Delta a}{c + \Delta c} \approx \frac{1 + \Delta a/a}{1 + \Delta c/a}. \quad (30)$$

For $\Delta c/a \ll 1$, then, $1/(1 + \Delta c/a) \approx 1 - \Delta c/a$. Thus,

$$\begin{aligned} \frac{a_{\text{new}}}{c_{\text{new}}} &= \left(1 + \frac{\Delta a}{a} \right) \left(1 - \frac{\Delta c}{a} \right) \\ &\approx 1 + \frac{\Delta c}{a} \left(\frac{\Delta a}{\Delta c} - 1 \right) = 1 + \frac{\Delta c}{a} \left(\frac{F_x}{F_z} - 1 \right) \end{aligned} \quad (31)$$

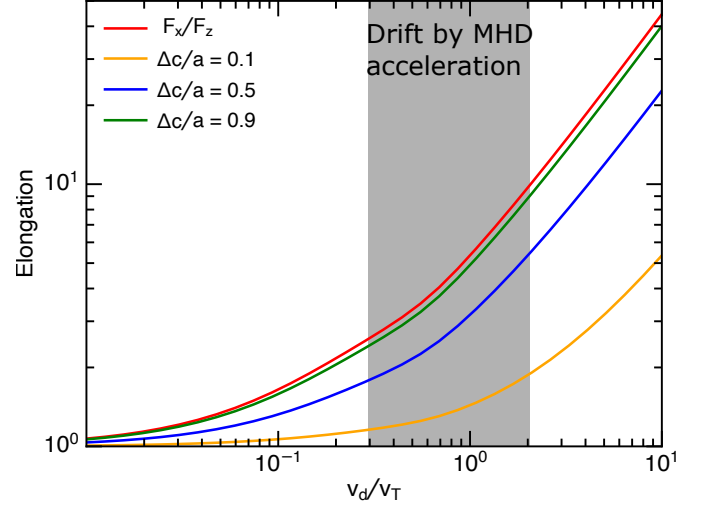


Figure 5. The ratio of the collision rate F_x/F_y and the grain axial ratio as function of v_d/v_T when the grain radius is increased by $\Delta c/a = 0.1, 0.5$ and 0.9 . Transonic and supersonic grains become highly elongated with elongation greater than ~ 3 by the time the grain size accumulates 50% of its radius.

It can be seen that for $v_d = 0$, the axial ratio is kept constant. For $v_d > 0$, the axial ratio increase because $F_x/F_z > 1$. By the time that the gas accretion increases the grain size by $\Delta c = a$, the axial ratio is increased to $a_{\text{new}}/c_{\text{new}} = (F_x/F_z)$.

Figure 5 shows the increase of the grain elongation with the drift velocity at three epochs when the grain accumulates a surface layer of 10, 50, 90% of its original radius. Transonic and supersonic grains become highly elongated with axial ratio of $a_{\text{new}}/c_{\text{new}} > 2$ by the time the grain size accumulates 50% of its radius. For the silicate grain in MCs accelerated by MHD turbulence with $v_d \sim 0.5 \text{ km s}^{-1}$ (see Table 1) or $s_d \sim v_d/v_T \approx 1$, Figure 5 implies an elongation of $a/c \approx 3$ and 5 by the time its radius increases by 50% and 90%, respectively.

5. GRAIN COAGULATION FROM DRIFTING ALIGNED GRAINS

5.1. Grain coagulation by collisions

The mean time between two successive collisions of two equal-size grains is given by

$$\begin{aligned} \tau_{\text{gg}} &= \frac{1}{\pi a^2 n_{\text{gr}} v_{\text{drift}}} = \frac{4\rho a M_{g/d}}{3n_H m_H v_{\text{drift}}} \\ &\simeq 7.6 \times 10^4 \hat{\rho} a_{-5} n_3^{-1} v_{\text{drift},1}^{-1} \text{ yr}, \end{aligned} \quad (32)$$

where n_{gr} is the number density of dust grains, $M_{g/d} = \mu n_H m_H / n_{\text{gr}} m_{\text{gr}} = 100$ with $m_{\text{gr}} = 4\pi a^3 \rho / 3$ is the gas-to-dust mass ratio, and we have assumed the single-grain size distribution.

Table 2. Timescales of grain alignment and grain growth of aligned grains

Parameters	Typical Values
Barnet relaxation (paramagnetic), $\tau_{\text{Bar}}(\text{yr})$	$0.5\hat{\rho}^2 a_{-5}^7 \hat{s} \left(\frac{1+\hat{s}^2}{2}\right)^2 \left(\frac{\omega_d}{\omega}\right)^2 \left[1 + \left(\frac{\omega\tau_2}{2}\right)^2\right]^2$
Nuclear relaxation, $\tau_{\text{nucl}}(\text{s})$	$610\hat{\rho}^2 a_{-5}^7 \left(\frac{n_e}{n_n}\right) \left(\frac{\omega_d}{\omega}\right)^2 \left(\frac{g_n}{3.1}\right) \left(\frac{2.7\mu_N}{\mu_n}\right) \left[1 + (\omega\tau_n/2)^2\right]^2$
Barnet relaxation (superparamagnetic), $\tau_{\text{Bar,sp}}(\text{yr})$	$3.2\hat{\rho}^2 a_{-5}^7 \frac{1}{N_{\text{cl}}} \left(\frac{\omega_d}{\omega}\right)^2 \times \left[1 + \left(\frac{\omega\tau_{\text{sp}}}{2}\right)^2\right]^2$
Paramagnetic relaxation, $\tau_{\text{mag}}(\text{yr})$	$2.4 \times 10^6 \hat{\rho} \hat{s}^{-2/3} a_{-5}^2 \left(\frac{B}{5\mu\text{G}}\right)^{-2} \left(\frac{10^{-13}\text{s}}{K(\omega)}\right)$
Superparamagnetic relaxation, $\tau_{\text{mag,sp}}(\text{yr})$	$2.4 \times 10^6 \hat{\rho} \hat{s}^{-2/3} a_{-5}^2 \left(\frac{B}{5\mu\text{G}}\right)^{-2} \left(\frac{10^{-13}\text{s}}{K_{\text{sp}}(\omega)}\right)$
Larmor precession, $\tau_{\text{Lar}}(\text{yr})$	$8.4\hat{\rho}^{-1/2} \hat{\chi}^{-1} \hat{B}^{-1} a_{-5}^2 \text{ yr}$
Gas damping time, $\tau_{\text{gas}}(\text{yr})$	$8.3 \times 10^3 a_{-5} \hat{\rho} \left(\frac{1}{n_3 T_1^{1/2}}\right)$
Gas accretion time, $\tau_{\text{acc}}(\text{yr})$	$1.2 \times 10^6 \frac{\hat{\rho} a_{-5}}{n_3 T_1^{1/2} X_{-2}}$
Grain-grain collision, $\tau_{\text{gg}}(\text{yr})$	$7.6 \times 10^4 \hat{\rho} a_{-5} n_3^{-1} v_{\text{drift},1}^{-1}$
External alignment (RAT) time, $\tau_{\text{RAT}}(\text{yr})$	$2 \times 10^3 \frac{a_{-5} n_3^{-1} T_1^{1/2}}{(\omega_{\text{RAT}}/3\omega_T)}$

The shattering threshold is $v_{\text{shat}} \sim 2.7 \text{ km s}^{-1}$ for silicate and 1.2 km s^{-1} for graphite grains (Jones et al. 1996; Yan et al. 2004). At high velocity produce shock waves inside the grains and shatter them in smaller fragments. Grain velocities in MC and DC are $v_d < v_{\text{shat}}$. therefore, grain shattering does not occur in the MC and DC. However, whether grains of $v < v_{\text{shat}}$ stick upon collision is unclear, and in MCs the presence of ice mantles is expected to enhance sticking collisions due to its larger threshold v_{cri} . Therefore, in this paper, we assume that sticky collisions and grain coagulation occur whenever $v < v_{\text{shat}}$.

Table 2 summarize the characteristic timescales involved in grain alignment and grain growth. The accretion and grain-grain collision time are much shorter than the internal alignment time (Barnett relaxation) and external alignment processes (Larmor precession and RAT alignment). As shown, the alignment time by RATs is at most $\tau_{\text{RAT}} \sim \tau_{\text{gas}}$, which is equal to the time required to collide with the gas of the same mass as the dust grain. Since the dust mass is 1 percent of gas mass, the grain collision time is 100 times longer. Note that the collision time between the grain size a with a tiny grain is shorter due to its higher density. However, such collisions do not randomize significantly the grain orientation because of its lower mass. Therefore, we can assume that aligned grains can be rapidly re-aligned before hitting another grain.

5.2. Nonaligned-nonaligned grains: stick and disalign

Consider first the collisions between randomly oriented grains. In this scenario, grain collisions are similar to what is studied previously. Figure 6 illustrates

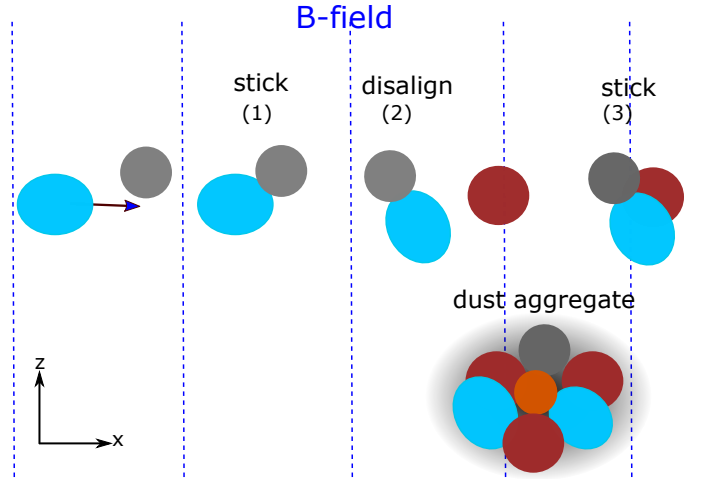


Figure 6. Illustration of coagulation by collisions of randomly oriented grains moving perpendicular to the mean magnetic field. After the first collision, grains stick and form an elongated grain (stage 1). The orientation of the resulting binary is randomized by gas collisions (stage 2), and then experiences the next collision along the direction with maximum cross-section, resulting in the large grain (stage 3) and eventually a dust aggregate.

the grain coagulation by collisions of non-aligned grains moving perpendicular to the mean magnetic field. After the first collision, grains stick and form an elongated binary. The newly formed grain is rapidly randomized by gas collisions, and then experiences the next random collision with the high probability along the direction with maximum cross-section. Therefore, coagulation of non-aligned grains leads to a dust aggregate of low elongation.

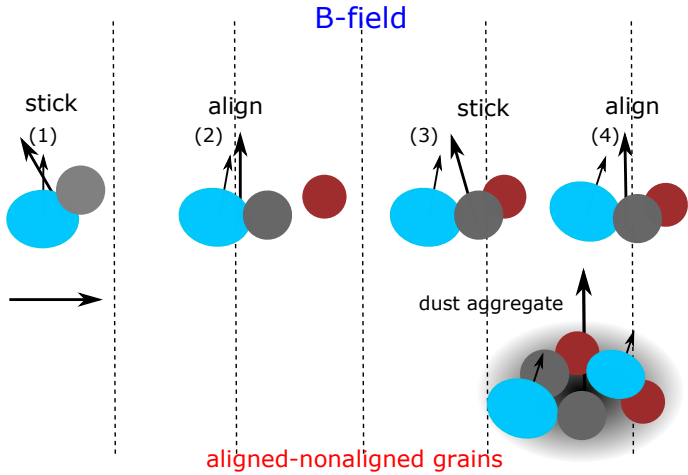


Figure 7. Illustration of grain coagulation by collisions of aligned-unaligned grains moving perpendicular to the mean magnetic field. The short arrow denotes that short axis of the aligned grain, and the long arrow denotes the short axis of the composite grain. After the first collision, the grains stick to become a binary (stage 1). The resulting elongated grain is rapidly aligned with the long axis perpendicular to the magnetic field (stage 2). The subsequent collision occurs along the long axis, results in the more elongated grain shape (stage 3), and becomes aligned with the magnetic field (stage 4). Finally, a dust aggregate is formed.

5.3. Aligned-nonaligned grains: stick and aligned

We now consider coagulation by collisions between an aligned grain with another nonaligned grain. Figure 7 illustrates the coagulation of one aligned grain with nonaligned grains. After sticking collisions, the monomers stick to become a binary (stage 1). If the collision results in the sudden disalignment so that the long axis deviates significantly from the angular momentum parallel to the magnetic field, then, internal relaxation rapidly bring the grain axis to be aligned with the magnetic field, provided that the particle size is smaller than $a_{\max, \text{int}}$ (see Figure 4). Note that the alignment timescale is shorter than the grain collision time τ_{gg} (see Table 2). Thus, the resulting elongated binary can be rapidly realigned with the long axis perpendicular to the magnetic field (stage 2). The subsequent collision occurs along the long axis, resulting in a more elongated particle (stage 3), and the re-alignment occurs due to internal relaxation and RAT alignment (stage 4). A dust aggregate is finally formed. Moreover, in the RAT paradigm, the nonaligned grain is smaller than aligned grains, so the collision would not result in a significant deviation of the net grain angular momentum from the magnetic field.

5.4. Aligned-aligned grains: stick and aligned

Figure 8 illustrates the coagulation from collisions between two aligned grains. After the first collision, a

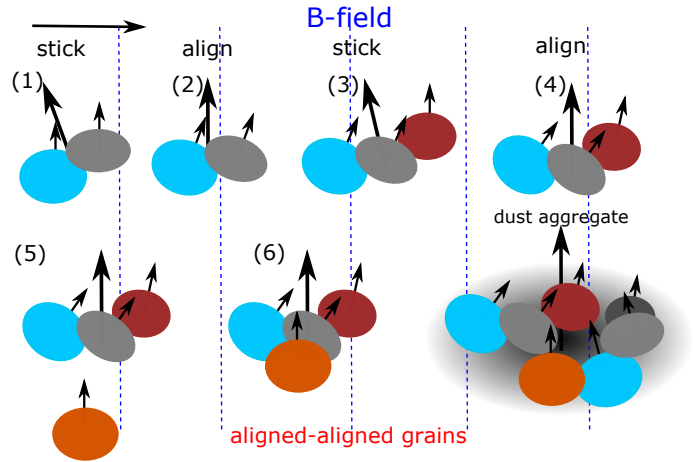


Figure 8. Same as Figure 7 but for collisions of aligned-aligned grains. The composite grain consists of elongated monomers with short axes (short arrows) parallel, and the short axis of the composite grain (long arrow) is directed along the magnetic field. Finally, a dust aggregate is formed that contains elongated grains with parallel short axes.

binary is formed and comprises a pair of aligned grains with parallel minor axes (short arrows). The minor axis of the binary (long arrow) is not necessary parallel to the grain's axes and makes a small angle (stage 1). However, internal relaxation rapidly brings the binary axis to be aligned with the magnetic field (stage 2). The first binary continues to collide with another aligned grain and coagulates, but the minor axes of the binary are slightly tilted from the third grain's axis (stage 3). The resulting particle has the short axis titled from the magnetic field and the angular momentum. The internal relaxation again acts to bring the internal alignment on a timescale of τ_{Bar} (stage 4). An aligned grain moving along the magnetic field can collide with the large grain and forms a dust particle (stage 5), subsequently relaxation processes bring it to be aligned with the magnetic field (stage 6). A dust aggregate is finally formed. The short axis of the dust aggregate is tilted by some small angle with the minor axes of the first binary. Thus, the coagulation from aligned grains leads to the formation of composite dust aggregates that contains elongated binaries made of oblate spheroids with parallel short axes inheriting from grain alignment with the magnetic field. The short axis of the dust aggregate is aligned along the magnetic field.

Figure 9 presents the coagulation of grains with wrong alignment with long axis parallel to the magnetic field. The process is similar to coagulation of aligned grains in Figure 8, but the first binary is made of two aligned grains with parallel long axes. The final dust aggregate

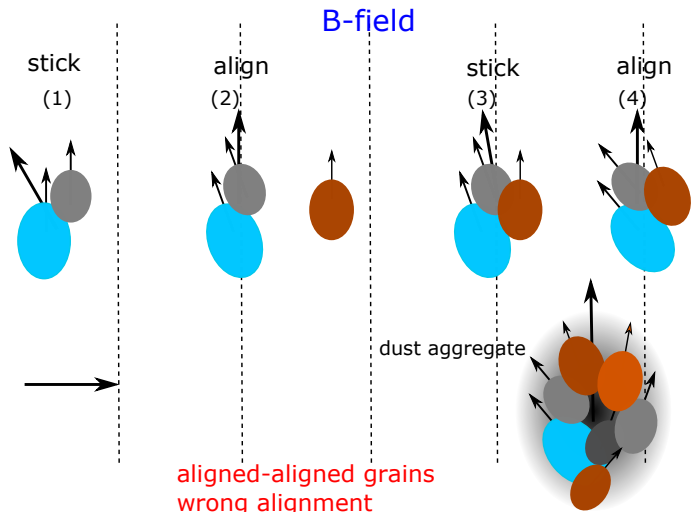


Figure 9. Same as Figure 8 but for grains with inefficient internal alignment and wrong alignment with long axis parallel to the spinning axis. Finally, a dust aggregate is formed that contains elongated grains with parallel long axes, and the long axis of the aggregate is parallel to the magnetic field due to wrong alignment.

contains aligned grains with parallel long axes and has its long axis parallel to the magnetic field.

6. DISCUSSION

6.1. Grain shape and structures from coagulation of aligned grains

We have studied the effect of grain alignment and motion across the magnetic field on grain growth by gas accretion and coagulation. For grains aligned with the short axis parallel to the magnetic field, the flux of gas species arriving along the direction of grain motion is increased significantly compared to the particle flux in the perpendicular direction (Figure 5). As a result of gas accretion, the shape of grains becomes oblate spheroidal due to fast rotation of the grain around the magnetic field. In addition, the grain elongation by gas accretion increases over time and become extremely elongated of elongation > 5 if the grain moves supersonically through the gas.

Coagulation from collisions between aligned grains first produces a binary comprising two aligned grains of oblate shapes with parallel short axes. The binary grains can be rapidly aligned by efficient internal relaxation and RATs, and then continues to collide with another aligned grain, forming a bigger particle with aligned axes. The grain growth process continues and eventually forms a micron-sized composite dust aggregate (Dominik & Tielens 1997; Ormel et al. 2009). Therefore, the dust aggregate contains elongated binaries of

two aligned particles with different sizes and orientations, forming a hierarchy structure.

Due to the rapid decrease in the efficiency of internal relaxation by Barnett effect with the grain size, as a^7 (see Eq. 5), there exists a maximum grain size that still has efficient internal alignment, $a_{\max, \text{Bar}}$. Thus, the largest size of an aligned binary within the dust aggregate is described by $a_{\max, \text{int}}$, which depends on dust magnetic properties and the gas density of the environment when grain growth occurs. For dense MC of $n_{\text{H}} \lesssim 10^5 \text{ cm}^{-3}$, dust of ordinary paramagnetic material has the $a_{\max, \text{int}} \sim 1 - 2 \mu\text{m}$, but it can increase to $5 - 10 \mu\text{m}$ for superparamagnetic grains with $N_{\text{cl}} \sim 10^4$ iron atoms per cluster (see Section 3). For the interior of PPDs of $n_{\text{H}} \gtrsim 10^{10} \text{ cm}^{-3}$, the maximum size of aligned grains is only $a \sim 0.7 \mu\text{m}$ (see Figure 4).

For grains larger than $a_{\max, \text{int}}$, internal relaxation is not efficient to align the grain short axis with the magnetic field, but it may induce the wrong alignment with the short axis perpendicular to the magnetic field. In this case, dust aggregates may contain the aligned grains with parallel long axes due to grain-grain collisions.

In the diffuse ISM, large grains of highly elongated shapes and structures are found to be disrupted by centrifugal stress due to grain fast rotation by RATs (Hoang et al. 2019; Hoang 2019; see Hoang 2020 for a review). This process removes highly elongated shapes and leaves behind the less extreme grain shapes.

6.2. Implications for polarization observations toward dense MC

Our study implies that grain growth from aligned grains has the elongation increasing from the diffuse ISM to MCs because the denser region has a higher growth rate, and the elongation can be large of $\epsilon > 3$ (see Figure 10). Therefore, the polarization cross-section efficiency (or intrinsic polarization efficiency) would increase toward denser environments as long as grains are still aligned. Assuming the perfect alignment of grains with the magnetic field, then the maximum level of thermal dust polarization would increase and can be larger than the maximum level of 19.8% measured by *Planck* satellite (Planck Collaboration et al. 2015a). Interestingly, high-resolution polarimetric observations of protostellar disks with *ALMA* report the maximum polarization level of 30 – 40% (Kwon et al. 2019; see Table 1 in Gouellec et al. 2020).

Observations of dust polarization in far-infrared and submm wavelengths usually reveal the decrease of dust polarization with increasing the visual extinction or column gas density. One explanation is that grains become less elongated toward dense regions due to grain growth

(e.g., Juárez et al. 2017). Such an explanation is expected for grain growth by gas accretion on randomly oriented grains because of the isotropic Brownian motion of thermal gas. However, our present study suggests that gas accretion to aligned grains makes the grain more elongated. Therefore, the origin of the polarization hole toward dense starless clouds is most likely caused by the loss of grain alignment by RATs, as shown in Hoang et al. (2021).

6.3. Coagulation of aligned grains in PPDs and implications for cometary dust

Comets form out of dust, ice, and gas beyond the snowline in PPDs, and thus, cometary dust aggregates contain valuable information about the coagulation process. However, where the growth from submicron sized grains to micron-sized dust aggregates starts, in PPDs or early phase of MCs, is uncertain.

Suppose grain coagulation to micron-sized begins in MCs. In that case, it involves grains aligned with the magnetic field, and thus, produces an elongated binary comprising two aligned grains parallel short axes embedded within a dust aggregate. This fundamental structure represents the earliest phase of grain growth where the environment is still not dense enough and grains can still be aligned. The elongated binary with axially aligned grains would be imprint in cometary dust particles. Moreover, the elongation of dust grains resulting from gas accretion and coagulation should increase with the grain size. Since aligned grains require paramagnetic and superparamagnetic inclusions, the aligned binary and elongated grains would contain a high level of iron.

Suppose grain growth mainly occurs in the disk midplane of PPDs. In that case, only small grains of $a < a_{\text{max,int}} \lesssim 0.7 \mu\text{m}$ can have internal alignment (see Figure 4), while larger grains with wrong internal alignment will lead to the dust aggregate made of aligned grains with parallel long axes. The orientation of the alignment axis in dust aggregates thus reveals unique information about where dust growth occurs.

Carbonaceous grains are not aligned with the magnetic field. Although carbonaceous grains can still move across the magnetic field, due to their random orientation, their shapes resulting from gas accretion is radically different from silicate grains, with elongation decreases over time. If interstellar dust is reprocessed and grows by accretion, then carbonaceous grains would have smaller elongation than silicate grains if these populations are separate. As a result, the fundamental carbonaceous grains imprint in cometary dust would be less elongated than silicates. Carbonaceous grains

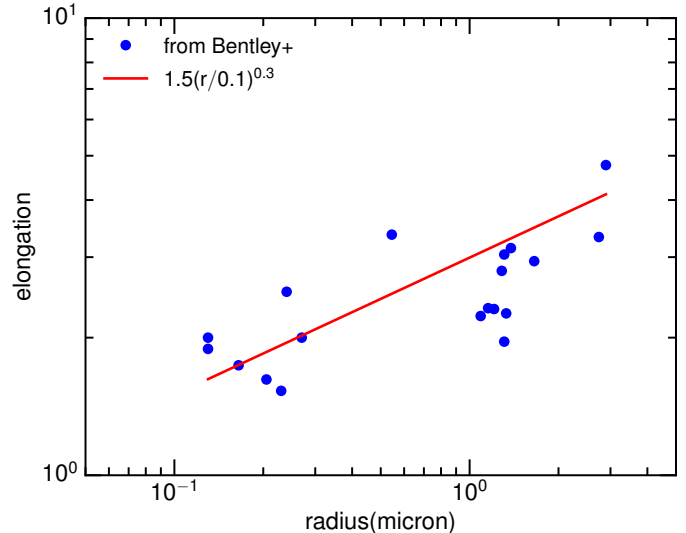


Figure 10. Elongation versus the grain radius of dust grains locked in dust from 67P/Churyumov-Gerasimenko comet from Bentley et al. (2016). The solid line shows the power-law of the elongation vs. the grain radius. The elongation tends to increase with the grain radius, which is consistent with the grain growth from aligned grains.

would produce binary structures with non-aligned axes. The identification of non-alignment of elongated carbonaceous grains would be a direct evidence for non-alignment of carbon.

Rosetta mission analyzed dust from 67P/Churyumov-Gerasimenko and found that cometary dust particles are aggregates of smaller, elongated grains of submicron sizes (Bentley et al. 2016). Figure 10 shows the variation of the fine grain elongation with grain radius of dust grains within dust aggregates using data from Bentley et al. (2016). The increase of the grain elongation with its radius (instead of decrease) implies that grain growth is not isotropic, as expected from Brownian motion. Nevertheless, it is consistent with grain growth from gas accretion and grain coagulation involving aligned grains. Further studies on the fundamental aligned structures and elongation of aligned grains within cometary and interplanetary dust aggregates are essential to test this scenario of grain growth.

7. SUMMARY

We study the effect of grain alignment with the interstellar magnetic field on grain growth due to gas accretion and grain-grain collisions. The main results are summarized as follows.

1. Charged grains in the ISM can be accelerated by gyroresonance by MHD turbulence, ambipolar diffusion, or shocks, and move in the direction perpendicular to the magnetic field.

2. In dense MCs of $n_{\text{H}} > 10^3 \text{ cm}^{-3}$, paramagnetic grains can have efficient internal alignment with the long axis perpendicular to the magnetic field for grain sizes of $a \lesssim a_{\text{max,int}} \sim 2 \mu\text{m}$. The inclusion of iron clusters can shift the range of internal alignment grains to $a_{\text{max,int}} \sim 10 \mu\text{m}$.
3. Grain alignment by RATs for grains of $a < a_{\text{max,int}}$ occurs with the long axis perpendicular to the magnetic field, which is thus parallel to the direction of grain motion. The grain alignment with the magnetic field occurs on a timescale shorter than grain growth time by gas accretion and coagulation, therefore, grain alignment should be considered for grain growth in MCs.
4. Fast rotation of the grain along the short axis (also magnetic field) leads to the oblate spheroidal shape for large grains that are grown by gas accretion to aligned elongated grains. The grain elongation by gas accretion increases over time and become extreme elongated of elongation > 5 if the grain moves supersonic through the gas.
5. Coagulation from aligned grains first produces a binary of aligned grains with parallel short axes and then to composite particles of oblate spheroid shapes due to the fast rotation around the magnetic field. The dust aggregates would contain a number of elongated binary comprising two aligned grains with parallel short axes.
6. Elongation of grains formed from coagulation of aligned grains should be larger than that formed from non-aligned grains. This is opposite from grain growth in the case of randomly oriented grains that makes the grain less elongated because the newly formed outer layer is isotropic. Due to their non-alignment with the magnetic field, carbonaceous grains would have lower elongation than silicate grains or grains with iron inclusions.
7. The orientation of elongated grains within a dust aggregate of cometary dust would provide information about where grain growth begins. Parallel short (long) axes of aligned grains imply that dust aggregates are formed in MCs or the surface layer of PPDs (disk midplane) where grains are internally aligned. A random orientation of elongated grains implies that grain growth occurs in very dense, shielded regions where grains are not aligned due to high density and lack of radiation field.
8. Grains within dust aggregates in 67P/Churyumov-Gerasimenko studied by *Rosetta* have the elongation increasing with the grain radius, which implies that such dust aggregates form by coagulation of aligned grains.

ACKNOWLEDGMENTS

T.H. acknowledges the support by the National Research Foundation of Korea (NRF) grants funded by the Korea government (MSIT) through the Mid-career Research Program (2019R1A2C1087045).

APPENDIX

A. FLUX OF GAS ACCRETION ONTO A DRIFTING ALIGNED GRAIN

Let $\hat{x}\hat{y}\hat{z}$ be the lab frame with $\hat{z} \parallel \mathbf{B}$. Let consider the grain drifting across the magnetic field with the velocity $\mathbf{v}_d = v_d \hat{x}$. Let $s_d = v_d/v_T$ with $v_T = (2kT_{\text{gas}}/m)^{1/2}$ is the thermal velocity of the gas specie of mass m .

The velocity distribution of gas in the lab frame is Maxwellian

$$f(v_x, v_y, v_z) d\mathbf{v} = f_x f_y f_z dv_x dv_y dv_z = Z^3 \exp\left(\frac{-mv^2}{2kT_{\text{gas}}}\right) dv_x dv_y dv_z \quad (\text{A1})$$

where $Z = (m/2\pi kT)^{1/2}$, and $\int_{-\infty}^{\infty} f(\mathbf{v}) dv_x dv_y dv_z = 1$.

In the grain's reference frame, the gas velocity is $v'_x = v_x - v_d, v'_y = v_y, v'_z = v_z$.

The flux of particles colliding with the upper surface of the grain along the z-direction is given by

$$\begin{aligned}
F_z &= \int_{-\infty}^{\infty} f_x dv_x \int_{-\infty}^{\infty} f_y dv_y \int_0^{\infty} n_H v_z f_z dv_z \pi a^2 \\
&= n_H \int_0^{\infty} Z v_z e^{-mv_z^2/2kT} dv_z = Z n_H \pi a^2 (2kT/m) \int_0^{\infty} Z e^{-x} dx / 2 = \frac{1}{2} n_H \left(\frac{m}{2\pi kT} \right)^{1/2} \frac{2kT}{m} = \frac{1}{2} n_H \left(\frac{2kT}{\pi m} \right)^{1/2} \\
&= \frac{1}{4} n_H \pi a^2 \langle v \rangle
\end{aligned} \tag{A2}$$

where $x = v_z^2/(2kT/m)$ and the lower limit is taken to be zero in order for the gas to hit the grain surface, and $\langle v \rangle = (8kT/\pi m)^{1/2}$ is the mean speed given by $\langle v \rangle = \int_0^{\infty} v \times 4\pi v^2 Z^3 e^{-mv^2/2kT} dv$.

Similarly, the collision rate by the gas onto one upper surface along the y-direction is given by

$$\begin{aligned}
F_y &= \int_{-\infty}^{\infty} f_x dv_x \int_{-\infty}^{\infty} f_z dv_z \int_0^{\infty} n_H f_y dv_y \\
&= \frac{1}{4} n_H \langle v \rangle
\end{aligned} \tag{A3}$$

Due to the grain motion, only the gas atom with velocity $v'_x = v_x - v_d < 0$ can collide with the grain. The collision rate to the front surface along the x-axis is

$$F_x = \int_{-\infty}^{\infty} Z \exp\left(-\frac{mv_y^2}{2kT}\right) dv_y \int_{-\infty}^{\infty} Z \exp\left(-\frac{mv_z^2}{2kT}\right) dv_z \int_{-\infty}^{v_d} dv_x n_H [-(v_x - v_d)] Z \exp\left(-\frac{mv_x^2}{2kT}\right), \tag{A4}$$

where the minus sign before $(v_x - v_d)$ accounts for the fact that the rate is positive. Performing the integral, one obtains

$$\begin{aligned}
F_x &= - \int_{-\infty}^{v_d} dv_x n_H (v_x - v_d) Z \exp\left(-\frac{mv_x^2}{2kT}\right) = n_H \pi a^2 \left(\frac{1}{4} \langle v \rangle e^{-mv_d^2/2kT} + \frac{v_d}{2} [1 + \text{erf}(v_d(m/2kT)^{1/2})] \right) \\
&= n_H \left(\frac{1}{4} \langle v \rangle e^{-s_d^2} + \frac{v_d}{2} [1 + \text{erf}(s_d)] \right)
\end{aligned} \tag{A5}$$

where $\text{erf}(\alpha) = \frac{2}{\sqrt{\pi}} \int_0^{\alpha} e^{-x^2} dx$. For $v_d = 0$, one sees that $F_x = \frac{1}{4} n_H \langle v \rangle$. For $v_d \gg v_T$, the first term becomes negligible and the second term goes to $n_H v_d$ because $\text{erf}(v_d \rightarrow \infty) \rightarrow 1$.

REFERENCES

- Barnett, S. J. 1915, *Physical Review*, 6, 239
- Bentley, M. S., Schmied, R., Mannel, T., et al. 2016, *Nature*, 537, 73
- Crutcher, R. M. 2010, *Highlights of Astronomy*, 15, 438
- Davis, L. J., & Greenstein, J. L. 1951, *ApJ*, 114, 206
- Dolginov, A. Z., & Mytrophanov, I. G. 1976, *Ap&SS*, 43, 257
- Dominik, C., & Tielens, A. G. G. M. 1997, *ApJ*, 480, 647
- Draine, B. T. 1996, in *Astronomical Society of the Pacific Conference Series*, Vol. 97, *Polarimetry of the Interstellar Medium*, ed. W. G. Roberge & D. C. B. Whittet, 16
- Draine, B. T., & Lazarian, A. 1999, *ApJ*, 512, 740
- Draine, B. T., & Weingartner, J. C. 1996, *ApJ*, 470, 551
- Gouellec, V. J. M. L., Maury, A. J., Guillet, V., et al. 2020, *A&A*, 644, A11
- Hall, J. S. 1949, *Science*, 109, 166
- Hiltner, W. A. 1949, *Nature*, 163, 283
- Hirashita, H., Il'in, V. B., Pagani, L., & Lefèvre, C. 2021, *MNRAS*, 502, 15
- Hirashita, H., & Li, Z.-Y. 2013, *MNRAS*, 434, L70
- Hirashita, H., & Yan, H. 2009, *MNRAS*, 394, 1061
- Hoang, T. 2019, *ApJ*, 876, 13
- Hoang, T. 2020, *Galaxies*, 8, 52
- Hoang, T., Cho, J., & Lazarian, A. 2018, *ApJ*, 852, 129
- Hoang, T., & Lazarian, A. 2008, *MNRAS*, 388, 117
- Hoang, T., & Lazarian, A. 2009a, *ApJ*, 697, 1316
- Hoang, T., & Lazarian, A. 2009b, *ApJ*, 695, 1457
- Hoang, T., & Lazarian, A. 2014, *MNRAS*, 438, 680
- Hoang, T., & Lazarian, A. 2016, *ApJ*, 831, 159

- Hoang, T., Lazarian, A., & Schlickeiser, R. 2012, *ApJ*, 747, 54
- Hoang, T., & Tram, L. N. 2019, *ApJ*, 877, 36
- Hoang, T., Tram, L. N., Lee, H., & Ahn, S.-H. 2019, *NAs*, 3, 766
- Hoang, T., Tram, L. N., Lee, H., Diep, P. N., & Ngoc, N. B. 2021, *ApJ*, 908, 218
- Jones, A. P., Tielens, A. G. G. M., & Hollenbach, D. J. 1996, *ApJ*, 469, 740
- Jones, R. V., & Spitzer, L. 1967, *ApJ*, 147, 943
- Juárez, C., Girart, J. M., Frau, P., et al. 2017, *A& A*, 597, A74
- Kwon, W., Stephens, I. W., Tobin, J. J., et al. 2019, *ApJ*, 879, 25
- Landau, L. D., & Lifshitz, E. M. 1969, *Mechanics* (Oxford: Pergamon Press)
- Lazarian, A. 2007, *J. Quant. Spectrosc. Rad. Trans.*, 106, 225
- Lazarian, A. 2020, *ApJ*, 902, 97
- Lazarian, A., Andersson, B.-G., & Hoang, T. 2015, in *Polarimetry of stars and planetary systems*, ed. L. Kolokolova, J. Hough, & A.-C. Levasseur-Regourd ((New York: Cambridge Univ. Press)), 81
- Lazarian, A., & Draine, B. T. 1999, *ApJ*, 520, L67
- Lazarian, A., & Hoang, T. 2007a, *MNRAS*, 378, 910
- Lazarian, A., & Hoang, T. 2007b, *ApJ*, 669, L77
- Lazarian, A., & Hoang, T. 2008, *ApJ*, 676, L25
- Lazarian, A., & Hoang, T. 2019, *ApJ*, 883, 122
- Martin, P. G. 1972, *MNRAS*, 158, 63
- Mathis, J. S., Mezger, P. G., & Panagia, N. 1983, *A& A*, 128, 212
- Morrish, A. H. 2001, *The Physical Principles of Magnetism* (Piscataway, NJ: IEEE Press)
- Ormel, C. W., Paszun, D., Dominik, C., & Tielens, A. G. G. M. 2009, *A& A*, 502, 845
- Planck Collaboration, Ade, P. A. R., Aghanim, N., Alina, D., & et al. 2015a, *A& A*, 576, A104
- Planck Collaboration, Ade, P. A. R., & Alves, M. I. R. e. a. 2015b, *A& A*, 576, A107
- Purcell, E. M. 1979, *ApJ*, 231, 404
- Vaillancourt, J. E., Andersson, B.-G., Clemens, D. P., et al. 2020, *ApJ*, 905, 0
- Wang, J.-W., Lai, S.-P., Eswaraiah, C., et al. 2017, *ApJ*, 849, 157
- Whittet, D. C. B., Bode, M. F., Longmore, A. J., Baines, D. W. T., & Evans, A. 1983, *Nature*, 303, 218
- Yan, H., & Lazarian, A. 2003, *ApJ*, 592, L33
- Yan, H., Lazarian, A., & Draine, B. T. 2004, *ApJ*, 616, 895